Research Article

MOLECULAR PAIN

Molecular Pain
Volume 15: 1–14

DOI: 10.1177/1744806918822185
journals.sagepub.com/home/mpx
SAGE

xCT knockdown in human breast cancer cells delays onset of cancer-induced bone pain

Robert G Ungard[1,2], Katja Linher-Melville[1,2], Mina Nashed[1,2], Manu Sharma[1,2], Jianping Wen[2], and Gurmit Singh[1,2]

Abstract

Cancers in the bone produce a number of severe symptoms including pain that compromises patient functional status, quality of life, and survival. The source of this pain is multifaceted and includes factors secreted from tumor cells. Malignant cells release the neurotransmitter and cell-signaling molecule glutamate via the oxidative stress-related cystine/glutamate antiporter, system x_C^-, which reciprocally imports cystine for synthesis of glutathione and the cystine/cysteine redox cycle. Pharmacological inhibition of system x_C^- has shown success in reducing and delaying the onset of cancer pain-related behavior in mouse models. This investigation describes the development of a stable siRNA-induced knockdown of the functional trans-membrane system x_C^- subunit xCT (*SLC7A11*) in the human breast cancer cell line MDA-MB-231. Clones were verified for xCT knockdown at the transcript, protein, and functional levels. RNAseq was performed on a representative clone to comprehensively examine the transcriptional cellular signature in response to xCT knockdown, identifying multiple differentially regulated factors relevant to cancer pain including nerve growth factor, interleukin-1, and colony-stimulating factor-1. Mice were inoculated intrafemorally and recordings of pain-related behaviors including weight bearing, mechanical withdrawal, and limb use were performed. Animals implanted with xCT knockdown cancer cells displayed a delay until the onset of nociceptive behaviors relative to control cells. These results add to the body of evidence suggesting that a reduction in glutamate release from cancers in bone by inhibition of the system x_C^- transporter may decrease the severe and intractable pain associated with bone metastases.

Keywords

pain, cancer-induced bone pain, nociception, breast cancer, system x_C^-, SLC7A11, glutamate, bone metastasis

Date Received: 25 September 2018; accepted: 29 November 2018

Introduction

Bone is the most common site of distant breast cancer metastases,[1] with an overall incidence of approximately 22% at or following diagnosis.[2] These metastases produce symptoms including severe and often untreatable pain that compromise patient functional status, quality of life, and survival[3] and can develop into a chronic pain condition.[4–6] Current management strategies of cancer-induced bone pain (CIBP) focus on radiotherapy and analgesic drugs including strong NSAIDs and opioids that induce severe dose-limiting side effects that are independently deleterious to treatment outcomes and patients' quality of life. As the number of cancer patients living with bone metastases increases, there is a growing need for interventions that focus on the preservation of quality of life.

Using animal models, cancer pain has been revealed to be a complex state with peripheral[7,8] and central[9–11] features of neuropathic and inflammatory pain. There are multiple potential mechanisms underlying the development and maintenance of CIBP, including direct

[1]Michael G. DeGroote Institute for Pain Research and Care, McMaster University, Hamilton, Ontario, Canada
[2]Department of Pathology and Molecular Medicine, McMaster University, Hamilton, Ontario, Canada

The first two authors contributed equally to this work.

Corresponding Author:
Gurmit Singh, Department of Pathology and Molecular Medicine, McMaster University, 1280 Main Street West, Hamilton, Ontario L8N 3Z5, Canada.
Email: singhg@mcmaster.ca

effects of tumor and stromal cells, as well as disrupted host bone cell processes. CIBP in animal models has been ameliorated by a number of promising approaches such as targeting inflammation,[12] acidosis,[13] and neurotrophin-induced neurogenesis.[7,14,15]

We previously demonstrated that human cancer cells with the capacity to metastasize to bone release glutamate through the cystine/glutamate antiporter system x_C^-.[16,17] System x_C^- exchanges glutamate for cystine, ameliorating oxidative/nitrosative stress arising from the accumulation of intracellular reactive species, which occurs due to altered metabolism of aggressive cancer cells. This cancer cell-derived glutamate accumulates in the bone where it can disrupt host tissues and activate and sensitize the Aβ-, Aδ-, and C-fibers sensitive to noxious mechanical, thermal, and chemical stimuli, all of which show changes in excitability in animal models of CIBP.[18] CIBP animal models demonstrate either a reduction or delay in the onset of nociceptive behaviors when treated with system x_C^--inhibitors sulfasalazine[19,20] and capsazepine[21] and when indirectly downregulated with peroxynitrate scavengers[20] and TrkA-inhibiting AG879.[22] This reduction in nocifensive behavior has been associated with extracellular glutamate levels in bone.[20]

We have developed a human MDA-MB-231 breast cancer cell line with a stable siRNA-induced knockdown of *SLC7A11*, the gene encoding the xCT transmembrane antiporter component of system x_C^-. This report describes the molecular and functional validation of this cell line in addition to RNAseq analysis to determine the transcriptomic consequences of xCT manipulation including changes in the expression of other pain-related factors. We also investigated the consequences of intrafemoral implantation of knockdown cells in a mouse model of CIBP to directly evaluate the system x_C^- as a potential therapeutic target in bone tumors. Rather than targeting the nervous system, this approach exploits a feature of the cancer cell itself to decrease nociception. This proof-of-principle study follows directly from previous work by our laboratory and others investigating pharmacological inhibition of system x_C^-,[19–22] and supports augmenting clinical pain management regimens with relevant system x_C^- blockers. This approach may reduce the requirement for increasing doses of centrally acting analgesics, such as opioids, that are currently prescribed to patients experiencing intractable CIBP, thereby improving quality of life.

Materials and methods

Cell culture

The human breast adenocarcinoma MDA-MB-231 cell line was used in all in vitro and in vivo work. Testing for mycoplasma contamination was performed throughout this study, and cells were verified to be mycoplasma-free prior to surgical implantation. All cells were maintained at subconfluent densities in a humidified incubator with 5% CO_2 in room air at 37°C using Dulbecco's Modified Eagle Medium (DMEM) supplemented with 10% fetal bovine serum and 1% antibiotic/antimycotic. Cell numbers were quantified in multiwell plates using crystal violet staining, measuring absorbance at $\lambda = 570$ nm with an optical plate reader (BioTek, Winooski, VT). Cell harvesting for in vivo implantation was performed on subconfluent cultures, and adherent cells were suspended and kept lightly agitated in sterile phosphate-buffered saline (PBS) on ice.

Knockdown cell generation

Stable system x_C^- knockdown breast cancer cells were generated using a shRNA approach with a puromycin-selectable mammalian expression vector carrying either a shRNA cassette specifically targeting the human xCT gene (*SLC7A11*) or an empty vector control.

MDA-MB-231 cells were transfected with four shRNA vectors: V2LHS-G1, V2LHS-C6, V3LHS-A12, and V3LHS-F12 (Open Biosystems, Thermo Fisher Scientific, Waltham, MA) as well as a pLKO-1 empty vector control (Millipore-Sigma, Oakville, Canada), using Lipofectamine 2000 (Thermo Fisher Scientific) (2 μg shRNA + 10 μl lipofectamine 2000/well of six well plate). Puromycin (5 μg/mL) (Millipore-Sigma) was added to growth media for selection after 48-h transfection, and media was refreshed every two to three days until cell colonies were formed three to four weeks later. All cell colonies for each shRNA vector were pooled and proliferated sufficiently for further analysis. These stable knockdown cell lines were named G1, C6, A12, and F12, respectively, and are maintained under normal culture conditions with 1 μg/mL puromycin.

Quantitative real-time polymerase chain reaction

cDNA was prepared using Superscript III (Thermo Fisher Scientific) and oligo dTs using total RNA extracted from cultured cell pellets or subcutaneous tumor tissue with the Qiagen RNeasy mini kit (Qiagen, Hilden, Germany) treated with DNase (Thermo Fisher Scientific). Quantitative real-time polymerase chain reaction (qPCR) was carried out on a BioRad CFX Connect Real-Time System with SsoAdvanced Universal SYBR Green Supermix (Bio-Rad Laboratories, Hercules, CA). Primers specific to the human xCT gene, as well as relevant housekeeping gene primers to amplify either β-actin or RNA polymerase II, have been described previously (Table 1). The $2^{-[\Delta][\Delta]Ct}$ method was employed to calculate the

Table 1. Primers used for relative qPCR to validate RNAseq results.

Gene	Citation/primerbank ID	Primer sequence (5′ to 3′)	Reference gene
SLC7A11 (xCT)	Livak and Schmittgen[31] and Habib et al.[33]	FOR: CCTCTATTCGGACCCATTTAGT REV: CTGGGTTTCTTGTCCCATATAA	*β-actin, RPII-1*
CCND2	Zimmermann[24]	FOR: ACCTTCCGCAGTGCTCCTA REV: CCCAGCCAAGAAACGGTCC	*β-actin*
CPT1A	Zhen et al.[32]	FOR: CCTCCAGTTGGCTTATCGTG REV: TTCTTCGTCTGGCTGGACAT	*RPII-1*
CSF1	Zimmermann[24]	FOR: AGACCTCGTGCCAAATTACATT REV: AGGTGTCTCATAGAAAGTTCGGA	*β-actin*
GSTM3	Zimmermann[24]	FOR: TACCTCTTATGAGGAGAAACGGT REV: AGGAAAGTCCAGGTCTAGCTTG	*β-actin, RPII-1*
IL1A	27894329c2	FOR: AGATGCCTGAGATACCCAAAACC REV: CCAAGCACACCCAGTAGTCT	*β-actin*
IL1B	27894305c1	FOR: ATGATGGCTTATTACAGTGGCAA REV: GTCGGAGATTCGTAGCTGGA	*β-actin*
IL1R	27894331c1	FOR: ATGAAATTGATGTTCGTCCCTGT REV: ACCACGCAATAGTAATGTCCTG	*RPII-1*
IL1R1L	27894327c1	FOR: ATGGGGTTTTGGATCTTAGCAAT REV: CACGGTGTAACTAGGTTTTCCTT	*RPII-1*
MYC	Zimmermann[24]	FOR: GTCAAGAGGCGAACACACAAC REV: TTGGACGGACAGGATGTATGC	*β-actin*
NGF	70995318c1	FOR: GGCAGACCCGCAACATTACT REV: CACCACCGACCTCGAAGTC	*β-actin*
NGFR	295842401c1	FOR: CCTACGGCTACTACCAGGATG REV: CACACGGTGTTCTGCTTGT	*RPII-1*
SENP1	45505133c1	FOR: AGTGAACCACAACTCCGTATTC REV: AAAAGATCGGTCCAAATGTCCTT	*β-actin*
SLC1A3	Zimmermann[24]	FOR: AGCAGGGAGTCCGTAAACG REV: AGCATTCCGAAACAGGTAACTTT	*β-actin*
SLC25A1	Zimmermann[24]	FOR: TTCCCCACCGAGTACGTGAA REV: GTAGAGCAGGGAGCTAAGGC	*RPII-1*
Reference genes			
β-actin	Livak and Schmittgen[31]	FOR: GATGGGCGGCGGAAAATAG REV: GCGTGGATTCTGCATAATGGT	
RPII-1	Zhen et al.[32]	FOR: GAAACGGTGGACGTGCTTAT REV: TCTCCATGCCATACTTGCAC	

Note: The sequence of validated human primers and their corresponding housekeeping genes used in this study are listed, each with a melting temperature of 60°C. Citations are provided for previously published primers. Those not published previously were selected using PrimerBank (www.pga.mgh.harvard.edu/primerbank)[36] with the ID listed. Efficiency-tested pairing of a specific target to housekeeper gene (β-actin or RPII-1) is indicated. RPII: RNA polymerase II.

relative mRNA levels,[23] and results are presented as fold changes of the control.

Western blotting

Twenty-five to fifty micrograms of total cell lysates were loaded onto 10% polyacrylamide gels for SDS-PAGE electrophoresis followed by immunoblotting using an anti-xCT (Novus Biologicals, Littleton, CO) antibody and chemiluminescent signal detection. Stripped polyvinylidene difluoride membranes were reprobed with either anti-β-actin (13E5, #4970S; Cell Signaling Technology, Danvers, MA) or anti-calnexin (H-70, sc-11397; Santa Cruz Biotechnology, Dallas, TX) antibodies. IgG horseradish peroxidase secondary antibodies (Cell Signaling Technology) were used.

Radiolabeled 14C-cystine uptake

Uptake of 14C-cystine (0.5 μCi/mL; Perkin Elmer, Waltham, MA) was determined using a Beckman LS6000 liquid scintillation counter as described previously.[21] Each lysate from cells plated 24 h prior to performing the assay was run in duplicate for at least three independent experiments. Scintillation counts per minute were normalized to total protein, which was determined using the Bradford assay.

Glutamate assay

The level of glutamate released into the culture media by cells plated 24 h prior to collection was determined using a modification of the Amplex Red Glutamic

Acid/Glutamate Oxidase Assay Kit (Thermo Fisher Scientific) and read on a CytoFluor Series 4000 Fluorescence Multi-Well Plate Reader (PerSeptive Biosystems, Thermo Fisher Scientific) as described previously.[16] Data from at least three independent experiments were normalized to total protein or cell number.

Animal models

Four- to six-week-old female Balb/c *nu*/*nu* immunocompromised mice (Jackson Laboratories) were used for all xenograft experiments. Mice were sterile housed and maintained at 24°C with a 12-h light/dark cycle and access to autoclaved food and water ad libitum. All procedures were conducted according to the guidelines of the Committee for Research and Ethical Issues of the International Association for the Study of Pain[24] and guidelines established by the Canadian Council on Animal Care with ethical approval from the McMaster University Animal Research Ethics Board. Three days prior to cell implantation surgeries, mice were anaesthetized by isoflurane inhalation, and 21-day-release pellets containing 0.25 mg of 17β-estradiol (Innovative Research of America, Sarasota, FL) were implanted subcutaneously. Although MDA-MB-231 are estrogen receptor negative, estrogen receptors are found throughout bone and play a role in the regulation of bone remodeling. In previous experiments, 17β-estradiol delivered prior to cancer cell inoculation improved the consistency of tumor establishment subcutaneously and in bone.[19]

Subcutaneous tumor models

Mice for subcutaneous tumor models were injected at the rear right flank with 4×10^6 cancer cells suspended in 100 μL sterile PBS. Animals were randomly assigned to receive the implantation of C6 xCT knockdown cells (n = 3), A12 xCT knockdown cells (n = 3), or vector-only negative control cells (n = 3). Subcutaneous tumor growth was monitored by measuring tumor dimensions with digital calipers and calculated according to the hemi-ellipsoid equation: Volume (mm^3) = LWH(π/6). Tumor size was evaluated 3×/week, and animals were sacrificed on day 36 postinjection prior to ethical end point for tumor size. Tumor tissues were collected postsacrifice, snap-frozen in liquid nitrogen, and stored at −80°C.

CIBP models

Intrafemoral CIBP mouse model-induction procedures were performed as previously described.[19] Briefly, 25 μL of sterile PBS containing 4×10^6 cancer cells was percutaneously implanted into the distal epiphysis of the right femur of anaesthetized mice. Animals were randomly assigned by a random number generator to receive implantation of either C6 xCT knockdown cells (n = 9) or vector-only negative control cells (n = 9) on experimental day 0. Tumors successfully developed in n = 5 C6 xCT knockdown cell-bearing mice and n = 7 control cell-bearing mice; data from all other mice were excluded from the final results. All animals were sacrificed on day 30 postinjection prior to ethical behavioral end points.

Behavioral analysis

Mice were exposed to handling and behavioral testing equipment daily for a 1-week acclimation period and assigned individual identification prior to model induction. All behavioral testing was performed by the same observers who were blinded to group assignment throughout the duration of the study. Behavioral testing was performed three times prior to model induction to obtain baseline data and two to three days a week beginning on day 1 following model induction and continuing until end point. The tests performed include two tests for spontaneous pain behaviors: the Dynamic Weight Bearing (DWB) system (BioSeb, Vitrolles, France) and open-field limb use scale; and one test for elicited mechanical allodynia and hyperalgesia, the Dynamic Plantar Aesthesiometer (DPA) (Ugo Basile, Comerio, Italy). Open-field observational limb use scale is an operator-derived numerical representation of the use of the animals ipsilateral limb 5-min period of free ambulation (0: no use, 1: severe limp, 2: moderate limp, 3: slight limp, and 4: normal use).[22] The DWB apparatus allows the recording of weight and time distribution between all points of pressure of freely moving animals and is described in more detail in previous reports.[19] The movement of each animal was recorded in the DWB apparatus for 5 min/test, and recordings were manually validated with DWB software version 1.4.2.92 (BioSeb). Results were exported as a mean weight for each point of pressure across the validated experiment time. Postural disequilibrium of the animal could indicate an allodynic response to normal ambulation, and so a reduction in weight borne by the tumor-afflicted limb of the animal was accepted as evidence of an inability or aversion to utilize that limb, providing indirect evidence of nociception. The DPA apparatus measures the threshold force and time to paw withdrawal from a mechanical stimulus to the plantar surface of the animal paw and is described in more detail in previous reports.[19] DPA testing was performed four times at each of the hind paws of all animals on each testing day. Animals were first given a minimum of 5 min to acclimate to the testing chambers prior to any stimulation. Mechanical withdrawal threshold is expressed as the mean force of four measurements

acquired on each testing day. A reduction in force withstood by the tumor-afflicted limb was accepted as evidence of increased sensitivity, both allodynic and hyperalgesic in that particular limb, manifested as a reflexive or desired withdrawal from stimulus, and therefore as indirect evidence of nociception. DPA data are presented for the tumor-bearing ipsilateral hind limb only.

Radiograph lesion scoring

High-resolution radiographic scans of all mice were taken at end point with a Faxitron MX-20 X-ray system (Faxitron X-ray Co., Wheeling, IL) on Kodak MIN-R 2000 Mammography film (Eastman Kodak, Rochester, NY). The extent of osteolytic lesions in the ipsilateral femurs imaged as a loss of bone density by postmortem radiograph was scored using a custom four-point (0–3) scale of bone destruction described in detail previously.[19] The scale designations are as follows: (0) normal bone, no visible lesion; (1) minor loss of bone density, minimal lesion; (2) moderate to substantial loss of bone density, lesion limited to bone trabecula and cortex; and (3) substantial loss of bone density, lesion includes clear periosteal involvement or fracture.

RNA-sequencing

Twenty microliters of RNA at 100 ng/μL from three independent biological replicate RNA samples were isolated from separate passages of MDA-MB-231 vector-only negative control and C6 xCT knockdown cells for RNAseq. RNA quality was measured using the RNA 6000 Nano kit and a 2100 Bioanalyzer (Agilent Technologies, Santa Clara, CA). Library preparation was performed using the NEBNext Ultra Directional RNA Library Prep Kit for Illumina, with the Next Poly(A) mRNA Magnetic Isolation Module (New England Biolabs, Ipswich, MA) to enrich poly-A mRNA. Samples were sequenced on the Illumina HiSeq 1500 platform (Illumina, San Diego, CA) via HiSeq Rapid V2 chemistry with onboard cluster generation and 70 bp single-end reads at the Farncombe Metagenomics Facility, McMaster University. Details of the sample preparation were conducted as previously reported.[25,26]

Each biological replicate was split between two lanes to mitigate lane effects, with reads being subsequently combined during analysis using the Tuxedo protocol.[27] Analysis was carried out using a web-based platform, the Galaxy Project, as previously described.[25,26] Briefly, the FastQC tool, Tophat, Cufflinks, and Cuffmerge were applied to evaluate the quality of sequencing, align reads to the human GRCh38/hg38 assembly, create assembled transcripts, and create a transcriptome assembly, respectively. Cuffdiff was then used to assess the transcript abundance in fragments per kilobase of transcript per million mapped reads (FPKM) and to identify the differentially expressed genes (DEGs) by merging the transcriptome assembly with individual aligned reads created by Tophat. The false discovery rate-adjusted P value (q value) was set to > 0.05. The Bioconductor package CummeRbund for RStudio (version 0.99.467 44–46) was used to graphically visualize group and pairwise comparisons of Cuffdiff's output files, including a scatter plot, volcano plot, expression level plot, and heat map. The Lander/Waterman equation ($C = LN/G$) was applied to calculate the mean genome coverage: C denotes the coverage, G corresponds to genome/transcriptome length (for RNA-sequencing), L denotes the average read length, and N stands for the average number of reads.[28] The base coverage tool in Galaxy (https://toolshed.g2.bx.psu.edu/view/devteam/ basecoverage/b8a9e718caa3) was used to derive the total length of annotated transcripts executed on the most recent human genome assembly (GRCh38), which was applied to calculate coverage. DAVID, a web-based bioinformatics tool, was applied to perform ontological and Kyoto Encyclopedia of Genes and Genomes (KEGG) pathway enrichment analyses to functionally interpret gene sets.[29,30] The list of DEGs for each pairwise comparison obtained from RNA-sequencing was imported into the "functional annotation" tool, with *Homo sapiens* as the reference species. Enriched KEGG pathways and Gene Ontology Biological Processes terms were identified with the Expression Analysis Systematic Explorer (EASE) threshold (maximum EASE score/P value) set to a default of 0.1, which is used by DAVID to identify significant gene enrichment. Fold-enrichment representing the ratio of the proportion of input genes relative to the number of genes represented by a particular term or pathway within the reference human genome was also reported. qPCR was performed to validate RNA-sequencing results (see "Materials and Methods" section on qPCR above). For each of the 15 target genes selected for validation, pairwise comparisons were based on fold changes calculated for the C6 clone relative to control. To determine the experimental asymmetrically distributed standard error of the mean (SEM) for each mean, which is required to linearly represent data derived from an exponential analysis, SEMs derived from each ΔCT value were used to calculate upper and lower $2^{-\Delta\Delta CT}$ values.[31] Linear regression was used to test the overall correlation between RNAseq and qPCR results, with α set to 0.05.[32] See Table 1 for a list of validated human primers and their corresponding housekeeping genes, all with melting temperatures of approximately 60°C. Those not described previously[26,33–35] were

selected based on PrimerBank (www.pga.mgh.harvard.edu/primerbank).[36]

Statistical analyses

Results represent the mean ± the SEM of at least three independent replicates for each experiment. Statistical differences between relevant groups were established by either t test (denoted by stars) or one-way analysis of variance coupled with a Tukey's posttest (denoted by different letters). Results were considered significant at $P < 0.05$. Immunoblots depict a representative image of three independent experiments. All behavioral data were analyzed across treatment groups with multiple unpaired t tests and presented as mean ± SEM. Osteolytic lesion scores were compared by Kruskal–Wallis test. A power analysis was performed prior to in vivo experimentation based on DPA results as primary measurement with a type II error ($\beta = 20\%$) and a type I error ($\alpha = 5\%$). All analyses and charts were generated using GraphPad Prism 7 software (GraphPad Software, La Jolla, CA).

Results

C6 and A12 MDA-MB-231 cell clones express reduced xCT mRNA and protein and reduced membrane transport of glutamate and cystine by system x_C^- relative to negative control cells

Following selection by puromycin, G1, C6, A12, and F12 xCT shRNA vector-transfected cells were screened for knockdown of xCT and reduction of functional system x_C^- activity. G1 and F12 clones were removed from further screening for failing to show reduction in glutamate release at a preliminary stage. xCT mRNA levels, as measured by qPCR, were significantly downregulated in both C6 and A12 xCT knockdown cell clones relative to vector-only negative control MDA-MB-231 cells (Figure 1(a)). Western blotting revealed that xCT protein levels at 35 kDa were reduced in both C6 and A12 clones relative to the vector-only negative control (Figure 1(b)). To confirm that this downregulation had functional consequences in the activity of the system x_C^- transporter that could translate to an impact on the extracellular environment, glutamate release into the culture media and cellular cystine uptake from the extracellular environment (both mediated in cancer cells by system x_C^-) were measured in vitro. Uptake of 14C-radiolabeled cystine, important in maintaining cancer cell redox balance, was reduced in both C6 and A12 knockdown clones relative to the negative control (Figure 1(c)). Glutamate released into the culture media over 24 h, which is the corresponding membrane transport action of system x_C^-, was also reduced to approximately 0.5-fold of negative control, as measured by AMPLEX red (Figure 1(d)). This confirmed the validity of the C6 and A12 clones as a model of *SLC7A11*/xCT knockdown in MDA-MB-231 human cancer cells.

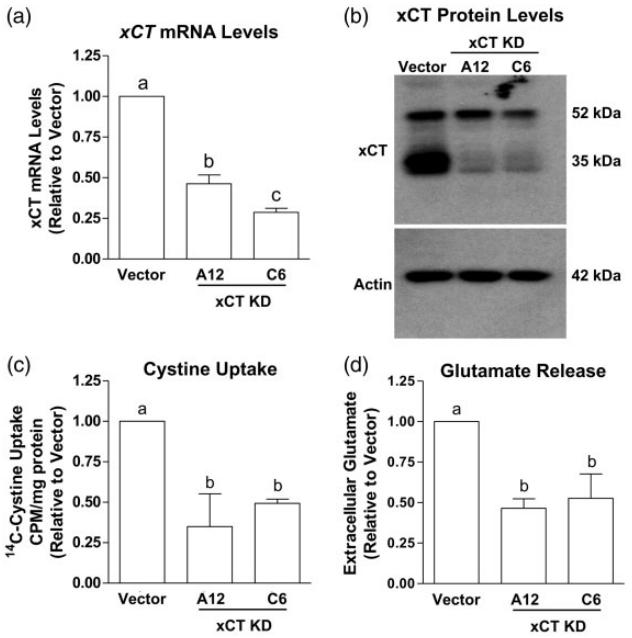

Figure 1. xCT mRNA and protein levels and system x_C^- functional cystine uptake and glutamate release are reduced in C6 and A12 xCT knockdown cell clones relative to vector-only negative control MDA-MB-231 in vitro. (a) xCT mRNA was significantly downregulated in both C6 and A12 xCT KD cell clones relative to vector-only negative control MDA-MB-231 cells (vector). xCT was also significantly lower in C6 than A12 xCT KD cells. (b) A representative Western blot image depicting that xCT protein levels at 35 kDa were lower in both C6 and A12 xCT KD cell clones relative to vector. Functional indicators of system x_C^- activity were reduced to approximately 0.5-fold of vector-only negative control cell activity in concordance with xCT expression levels. These include (c) 14C-radiolabeled cystine uptake and (d) glutamate release into culture media, both from cells in culture for 24 h. Data represent the mean of three independent experiments (±SEM) calculated relative to vector. Different letters a, b, or c in panels a, c, and d correspond to statistical differences between groups ($P < 0.05$), as determined by one-way analysis of variance and post hoc Tukey's test. KD: knockdown.

C6 cell clones retain xCT transcript and protein reduction in subcutaneous tumor tissue from mice 36 days following implantation

Prior to implantation in a mouse model of CIBP, it was necessary to determine whether these xCT knockdown cell lines could successfully induce a xenograft tumor in vivo in Balb/c *nu*/*nu* immunocompromised mice and to determine whether xCT downregulation was retained in tumor tissue following a period of in vivo growth without puromycin. C6 and A12 xCT

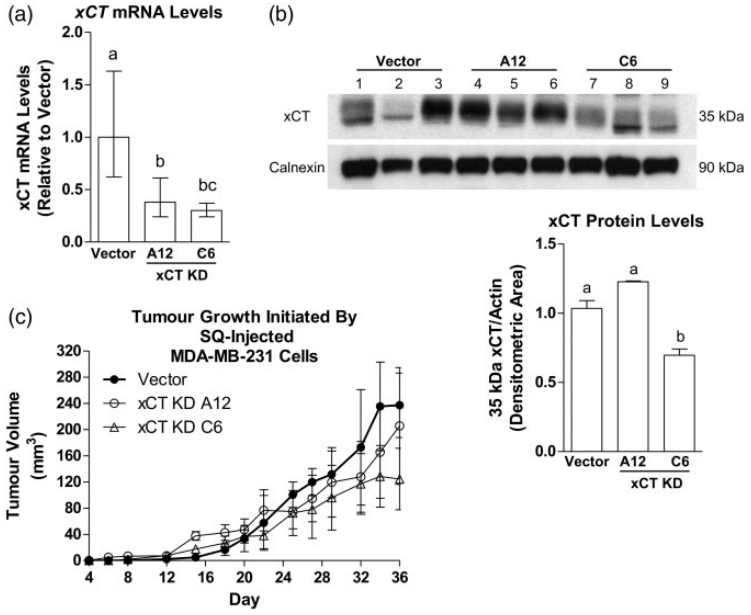

Figure 2. xCT mRNA and protein levels remain downregulated in subcutaneous tumor tissue from C6 xCT KD cells, while mRNA but not protein remains reduced in tumors from A12 xCT KD cell clones relative to vector-only negative controls. Subcutaneous tumors did not significantly differ in size. 4×10^6 C6 and A12 xCT KD cells and vector-only negative control MDA-MB-231 cells (vector) were implanted subcutaneously into nude mice ($n = 3$/group). Tumor tissue was collected after 36 days of growth. (a) xCT mRNA levels remained significantly downregulated in subcutaneous tumor tissue collected from both C6 and A12 xCT KD cell clones relative to vector. xCT was also lower in C6 than A12 xCT KD cell-derived tumors. (b) xCT protein at 35 kDa was also significantly lower in C6 but not A12 xCT KD cell clones relative to vector in tumors, as quantified by densitometric analysis of xCT protein levels relative to actin measured by Western blotting. (c) Tumor growth was measured throughout the duration of the experiment; at no point did tumor size (mm^3) significantly differ between groups as compared by one-way analysis of variance (ANOVA). Data represent the mean of three independent experiments (±SEM) calculated relative to vector. Different letters a, b, or c in panels a and b correspond to statistical differences between groups ($P < 0.05$), as determined by one-way ANOVA and post hoc Tukey's test. KD: knockdown.

knockdown cells and vector-only negative control MDA-MB-231 cells (4×10^6 cells/mouse) were implanted subcutaneously in mice ($n = 3$/group). Subcutaneous tumor tissues were removed at sacrifice after 36 days of in vivo growth and examined by qPCR for xCT mRNA and Western blotting for protein ($n = 3$/group). xCT mRNA was significantly downregulated in subcutaneous tumor tissue from the C6 and A12 xCT knockdown cell clones relative to negative control MDA-MB-231 cells (Figure 2(a)). Consistent with in vitro transcript results, xCT mRNA remained significantly lower in C6 clones than in A12 xCT knockdown tumor tissue. Western blotting for xCT protein at 35 kDa revealed that while xCT was significantly lower in tumor tissue from C6 clones, there were no differences between A12 clones and control cells, as quantified by densitometry (Figure 2(b)). Based on these results showing a robust and retained significant knockdown of xCT both in vitro and following in vivo growth in the C6 clone, further investigation including RNAseq and models of CIBP focused on this stable cell line. Tumor growth was measured throughout the duration of the experiment by calipers and reported as hemi-ellipsoid (mm^3), and while tumors exhibited variability, at no point did tumor size significantly differ between groups (Figure 2(c)).

RNAseq revealed DEGs in C6 xCT knockdown cell clones relative to vector-only negative control MDA-MB-231 cells

Gene expression from three biological replicates of C6 xCT knockdown cell clones and vector-only negative control MDA-MB-231 cells was compared by RNAseq. DEGs are highlighted in Figure 3, and the full list of DEGs is provided in Supplementary Table 1. Overall, gene expression similarities and differences between C6 xCT knockdown cell and negative control cells are indicated by scatter plot (Figure 3(a)). Volcano plotting highlights genes that were differentially expressed between C6 xCT knockdown cell and control cells by plotting −log10 (*P* value) against log2(fold change) of individual genes (Figure 3(b)). A density plot illustrates expression level

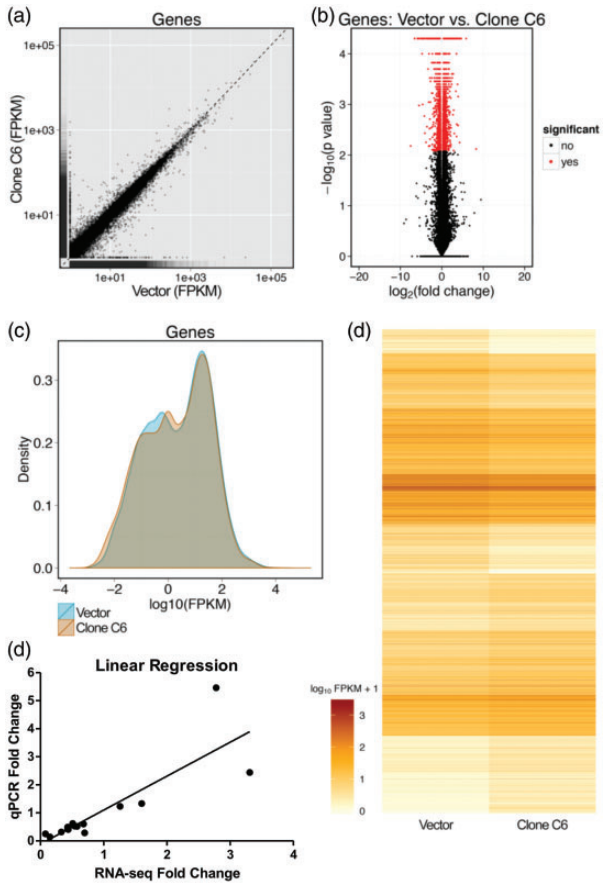

Figure 3. A visual summary of patterns of differentially expressed genes derived from RNA-sequencing of C6 xCT knockdown (KD) and vector-only negative control MDA-MB-231 cells. (a) Overall gene expression similarities and differences between C6 xCT KD cells and vector-only negative control cells (vector) are indicated by scatter plot. (b) Volcano plotting highlights genes that were differentially expressed between C6 xCT KD cells and vector. (c) A density plot illustrates expression level distribution, with non-overlapping segments representing differential gene expression between C6 xCT KD cells and vector. (d) Heat mapping illustrates the level of gene expression in log10(FPKM+1) for genes that are differentially expressed between C6 xCT KD cells and vector. (e) Linear regression analysis of qPCR results compared with RNAseq results revealed high concordance between the two methods. FPKM: fragments per kilobase of transcript per million mapped read; qPCR: Quantitative real-time polymerase chain reaction.

distribution, with nonoverlapping segments representing differential gene expression between C6 xCT knockdown cell and control cells (Figure 3(c)). Heat mapping illustrates the level of gene expression in log10(FPKM + 1) for genes that were differentially expressed between C6 xCT knockdown cell and control cells (Figure 3(d)). A complete list of DEGs is shown in Supplementary Table 1. Linear regression analysis of qPCR results compared with RNAseq results including a wide range of fold changes revealed high concordance between the two evaluations of gene expression (Figure 3(e)).

Fifteen DEGs identified by RNAseq across a range of fold changes and including cytokines, growth factors, and xCT were validated by quantitative real-time reverse transcription PCR (RT-qPCR)

xCT knockdown was confirmed by RNAseq and qPCR, and other DEGs identified by RNAseq representing a range of fold changes were validated by qPCR (Figure 4). These included *SLC7A11* (xCT), which was downregulated to less than 0.5-fold at $P < 0.05$, and genes of interest related to xCT expression and CIBP in cancer cells. *CCND2*, *CPT1A*, *CSF1*, *GSTM3*, *IL1A*, *IL1B*, *IL1R1*, *IL1R1L*, *NGF*, and *SLC1A3* were significantly upregulated or downregulated to a significance level of $P < 0.01$; *SENP1* was upregulated at $P < 0.05$; and *MYC*, *NGFR*, and *SLC25A1* were not significantly different between C6 xCT knockdown cell clones relative to the negative control as compared by *t* test.

C6 xCT knockdown cells implanted in bone produce a delayed development of pain-related behavior in mice relative to implantation of vector-only control cells

To determine whether the reduction in cancer cell expression of xCT and the corresponding decrease in system x_C^--mediated glutamate release from these clones had an impact on behaviors indicative of nociception, C6 xCT knockdown cells and vector-only negative control MDA-MB-231 cells (1×10^6 cells/mouse) were implanted intrafemorally in mice ($n = 9$/group). Tumors developed in $n = 5$ C6 cell-bearing mice and $n = 7$ vector-only control cell-bearing mice as verified by X-ray and hematoxylin and eosin staining. Animals implanted with C6 xCT knockdown cells displayed reduced or delayed behaviors indicative of nociception relative to vector-only MDA-MB-231 controls with normal xCT expression and system x_C^- function. Weight borne on the rear right ipsilateral limb as measured by DWB progressively declined in both groups as tumors grew in the bone. The onset of this decline was delayed in the C6 xCT knockdown group relative to control, groups were significantly different on experimental days 19 and 22 (Figure 5(a)). The decline in time of ipsilateral limb use was also delayed in the C6 clone group relative to control, with a significant difference between groups on day 19 (Figure 5(b)). Other measures recorded by the DWB apparatus including paw surface area and relative weight bearing also showed significant differences between groups at similar time points, as did reaction time as measured by DPA (data not shown). Both C6 xCT knockdown and control

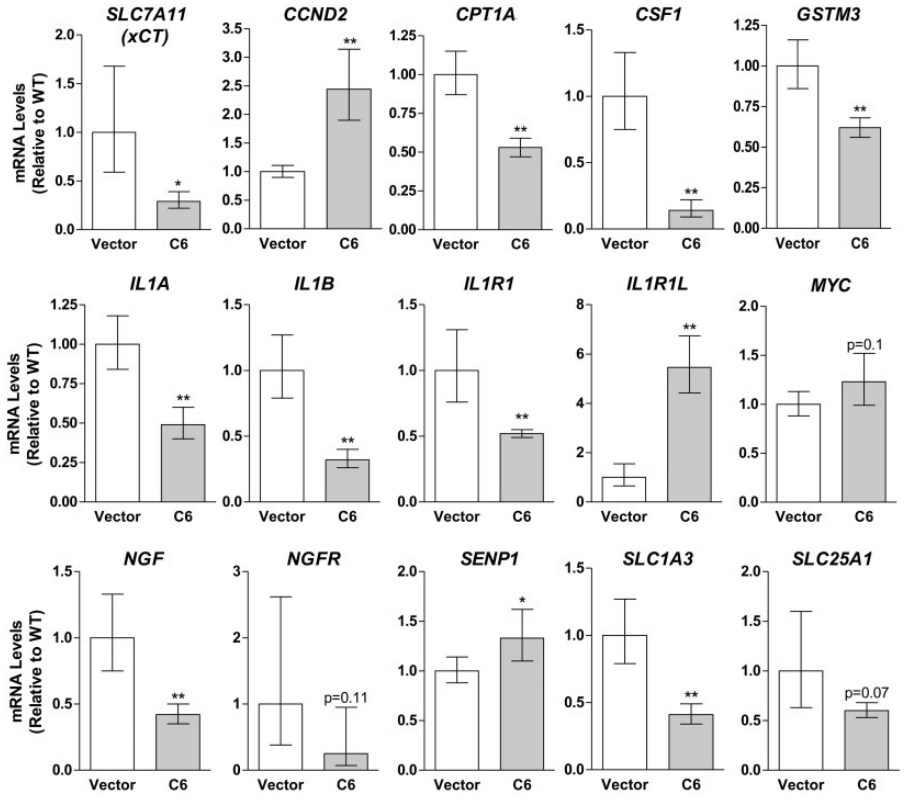

Figure 4. Fifteen genes selected for representation of relative qPCR fold changes and validation of differentially expressed genes (DEGs) identified by RNA-sequencing indicate differences between gene expression in C6 xCT knockdown (KD) cell and vector-only negative control cells. xCT KD was confirmed by RNAseq and qPCR, and other DEGs identified by RNAseq representing a range of fold changes were validated by qPCR. These include genes of interest related to xCT expression and CIBP in cancer cells. For each group, data represent the mean of three independent biological replicates, each analyzed in duplicate, with error bars indicating the SEM calculated using the $2^{-[\Delta][\Delta]Ct}$ method. Data of the C6 xCT KD clone are presented relative to vector (fold change). Means were compared using t tests (*$P < 0.05$, **$P < 0.01$). WT: wild type.

animal groups also demonstrate a decline in mechanical force (g) required to provoke ipsilateral paw withdrawal as measured by the DPA-automated von Frey test. This decline was delayed in the C6 xCT knockdown group (Figure 5(c)). Observational scoring of ipsilateral limb use (0–4 scale) also showed a later onset of nociceptive behavior in the C6 clone group relative to control (Figure 5(d)). No behavioral measures showed significant differences between groups at end point, indicating that this xCT-mediated decrease in nociceptive behaviors was not an overall reduction in nociception throughout the duration of the model, but a delay in the time-to-onset of severe nociceptive behavior. Osteolytic lesion sizes in the femur at end point as measured by radiograph were not different between groups (Figure 5(e)), indicating that these behavioral differences were related to differential cancer cell phenotype rather than overall tumor size. All behavioral data were confirmed for normal distribution and analyzed across treatment groups with multiple unpaired t tests and presented as mean ± SEM (*$P < 0.05$). Osteolytic lesion scores were compared by Kruskal–Wallis test.

Discussion

Cancer pain may arise from many factors, including weak and fractured bone, inflammation, neuropathy, and disruptive signaling via molecules released by a tumor or tumor-associated cells. The findings detailed in this report follow directly from findings by our laboratory and by the Vanderah laboratory that pharmacological inhibitors of system x_C^- reduce or delay the onset of pain behavior in mouse models of CIBP at least in part by reducing glutamate release from the cancer cell to the bone microenvironment.[19–22] By directly targeting the expression of SLC7A11/xCT in human cancer cells without the confounding off-target factors of systemic drug treatment, we have produced a cell and in vivo mouse model that can more directly evaluate the impact of targeting xCT and therefore system x_C^- activity for the treatment of cancer pain.

Bone cancers are more commonly the result of metastasis than of a primary cancer of the bone, and the breast is the most common site of origin of these metastases, with the majority of late-stage breast cancers producing

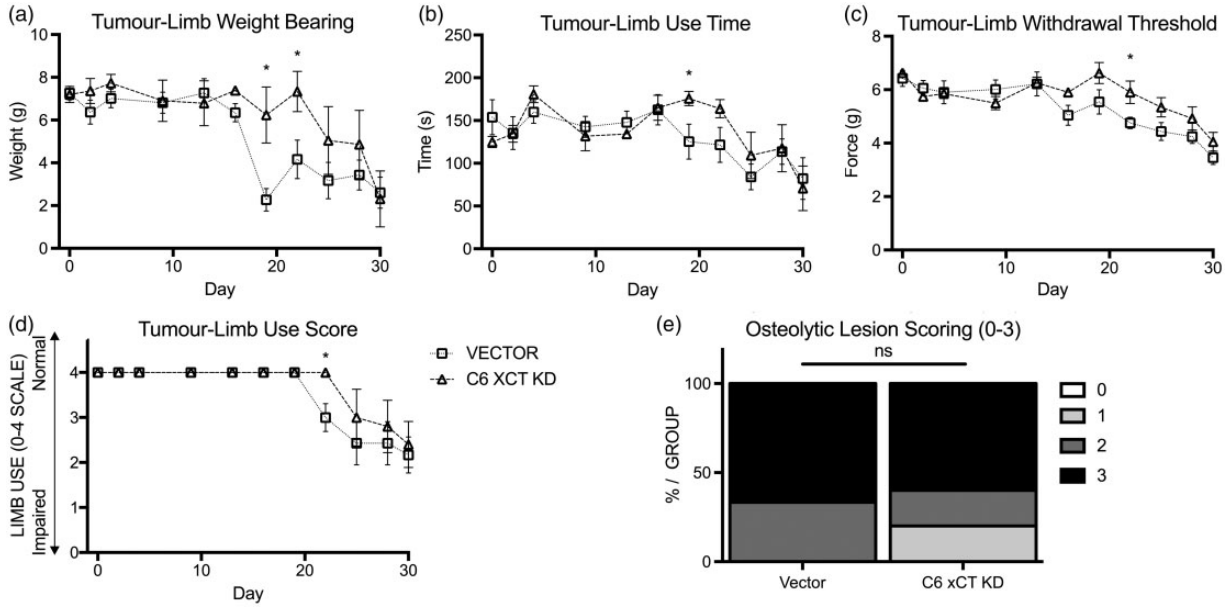

Figure 5. xCT KD in implanted bone tumors delays the development of nociceptive behavior in mice including measures of limb use and mechanical withdrawal threshold. When implanted intrafemorally to induce a mouse model of CIBP, animals with C6 xCT KD cells displayed reduced or delayed behaviors indicative of nociception relative to vector-only MDA-MB-231 controls (vector) with normal xCT expression and system x_C^- function. (a) Weight bearing on the rear right ipsilateral limb as measured by DWB progressively declines in both groups as tumors grow in the bone. The onset of this decline is delayed in the C6 xCT KD group relative to vector; groups are significantly different on experimental days 19 and 22. (b) The temporal decline of ipsilateral limb use is also delayed in the C6 clone group relative to control, with a significant difference between groups on day 19. (c) Both C6 xCT KD and vector animal groups also demonstrate a decline in mechanical force (g) required to provoke ipsilateral paw withdrawal as measured by DPA-automated von Frey. This decline is delayed in the C6 xCT KD group. Groups are significantly different on experimental day 22. (d) Observational scoring of ipsilateral limb use (0–4 scale) also shows a later onset of nociceptive behavior in the C6 xCT KD group relative to vector, with groups significantly differing on experimental day 22. In a to d, no measures show significant differences between groups at end point. (E) Osteolytic lesion size in the femur at end point was not different between groups. Data are reported from $n = 5$ C6 xCT KD cell mice and $n = 7$ vector cell mice; only animals with verified tumor development were included in results shown here. All behavioral data are presented as mean ± SEM analyzed across treatment groups with multiple unpaired t tests ($^*P < 0.05$). Osteolytic lesion scores were compared by Kruskal–Wallis test. KD: knockdown.

at least one metastatic site in the skeleton.[4,37] We chose to produce our stable xCT knockdown cell line in MDA-MB-231 triple-negative human breast adenocarcinoma which produce osteolytic lesions when implanted in bone and have been established by our laboratory for use in a mouse model of CIBP.[19,21] MDA-MB-231 are among many cancer cell lines from a range of tissues of origin that release glutamate via system x_C^-. However, this phenomenon has been most comprehensively examined in human triple-negative breast cancer cells, where xCT was found to be highly expressed in the majority of cell lines adapted to culture, and in 40% of a sample of patient-derived triple-negative breast tumor samples.[38] System x_C^- expression and activity have been implicated in cellular responses to oxidative stress, allowing enhanced cancer cell survival and acquired resistance to therapy,[39,40] supporting aberrant cancer cell metabolic processes including upregulated glutaminolysis.[26,41] In the bone, glutamate is implicated in cell signaling and regulation of osteoblasts, osteoclasts, and osteocytes.[42] Bone metastases can induce dramatic disruptions in bone cell metabolism which can increase and dysregulate processes of bone resorption and apposition, producing large and painful lesions.[43] Extracellular glutamate also has the potential to activate and sensitize glutamate-receptive peripheral sensory neurons including nociceptors in and around the bone.[41,44]

In vitro, two stable cell clones (C6 and A12) transfected with shRNA cassettes targeting *SLC7A11*/xCT, showed downregulated xCT at both the mRNA and protein levels, with significantly downregulated indicators of functional system x_C^-, including cystine uptake and glutamate release relative to a vector-only negative control. Following subcutaneous in vivo implantation and growth, C6 clones were selected for further investigation by RNAseq and for use in an animal model of CIBP, based on that clone's retention of approximately 50%

knockdown of xCT based on mRNA and protein levels relative to control cells. In addition, subcutaneous tumors from implanted C6 clone and negative control cells did not significantly differ in volume (mm^3) over the 30-day time period corresponding to the duration of the intrafemoral CIBP model. Although experimental interference with system x_C^- is often intended to reduce growth of or even kill cancer cells, this outcome could be a dramatic confound in our mechanistic investigation into the validity of xCT at a target for cancer pain. Consistency in tumor size allows a more isolated investigation of the direct impact of xCT and system x_C^--mediated glutamate release on CIBP.

In our CIBP model, we observed a delay between the onset of nociceptive behaviors in mice intrafemorally injected with negative control cells with normal xCT expression and later onset in C6 clone xCT knockdown cells. In particular, we observed a reduction in behaviors indicative of mechanical allodynia in C6 clone-bearing mice, including spontaneous ipsilateral weight bearing and time-of-use with the DWB, and evoked mechanical withdrawal threshold using the DPA test, which may also be indicative of mechanical hyperalgesia. We observed a reduction in spontaneous indications of limb use limitation or avoidance with the observational 0 to 4 scale, possibly indicating spontaneous allodynia. Other observational measures of spontaneous nociception including guarding time and flinching were found to be inconsistent or absent in Balb/c *nu*/*nu* mice. We hypothesize that this delay in the onset of nociceptive behaviors is a result of reduced glutamate release into the extracellular environment, where elevated levels of glutamate in the femur are associated with CIBP.[20] This time frame in a mouse model could represent a clinically relevant delay in potential targeting of xCT for CIBP in cancer patients, allowing not only a lesser overall experience of pain but also a delay until the need for stronger analgesic intervention. By end point, there were no behavioral differences between groups, and animals were sacrificed prior to reaching behavioral ethical end points, consistent with previous findings of pain amelioration by targeting system x_C^-.[19–22] This is indicative of the complexity of CIBP, a pain state that involves many initiating and maintaining factors apart from cancer cell-derived glutamate, including other secreted factors, mechanical distortion, and direct neuronal damage or pathology—processes that could induce pain independently of system x_C^- and glutamate.[45,46]

In rat models of intrafemoral tumors, we have observed plasticity in the intracellular electrophysiological characteristics of cutaneous and muscle spindle peripheral sensory neurons, including nociceptive C- and Aδ-fibers, as well as normally nonnociceptive Aβ-fiber low threshold mechanoreceptors.[18] These rat models demonstrated behavioral results similar to the current mouse models, including reductions in mechanical withdrawal threshold, and measures of ipsilateral limb use.[18] It is possibly the case that these same intrinsic membrane properties, including neuronal excitability, are altered in our mouse models of CIBP, with potentially relevant changes in particular fiber types resulting from system x_C^- inhibition, although in vivo intracellular recordings have yet to be performed in mice.

Changes in gene expression between C6 xCT knockdown cell clones and vector-only negative control cells as compared by RNAseq confirmed that *SLC7A11* mRNA levels were significantly downregulated in C6 cells. In addition, transcripts of other factors implicated in feedback with system x_C^- and pain, including *NGF*, which has a well-established relationship with cancer and skeletal pain,[7,22] as well as interleukin 1 beta (*IL1β*), which has been implicated in both xCT regulation[47,48] and cancer pain,[49,50] were also downregulated in C6 cells. In addition, the transcript encoding colony-stimulating factor 1 (CSF1), which modulates innate immunity, inflammation and cancer, as well as macrophage activation and the support of microglia,[51,52] was also significantly downregulated, along with its receptor *CSF1R* (to 0.4-fold via RNAseq) in the C6 xCT knockdown cells relative to controls at the mRNA level. Interestingly, in a T47D human mammary carcinoma cell line that overexpresses xCT and releases significantly more glutamate than wild-type T47D control cells, CSF1 levels are significantly increased by 2.5-fold.[26] C6 xCT knockdown clones also exhibited significant downregulation of *TNFRSF1A* (to 0.58-fold via RNAseq relative to control), which encodes the receptor for the pro-inflammatory cytokine tumor necrosis factor alpha (TNFα), which is also associated with cancer pain.[53] Our RNAseq data suggest that the xCT status of a bone tumor may be linked with other important pronociceptive players, and its downregulation may be beneficial not only by reducing glutamate levels but also through concomitant downregulation of neurotrophic factors and pro-inflammatory cytokines implicated in modulating the complex state of CIBP.

Our conclusions that xCT downregulation is associated with reduced CIBP in animal models and that xCT expression in cancer cells is linked with transcriptomic changes that include several other well-known players in the generation of cancer pain add to growing body of mechanistic CIBP research. Rationale is accumulating for the therapeutic targeting of xCT as a way to manipulate a metabolically unique feature of many cancers that may impact not only the cancer cell growth and survival but also the associated morbidities of cancer including pain, seizures,[54] and depression.[55] Our findings are consistent with the role of xCT in cancer and cancer pain. We intend to further evaluate the mechanisms and consequences of xCT manipulation in cancer cells by

producing an inducible xCT knockdown system to strategically silence expression of the antiporter in a temporally controlled manner and to evaluate the contribution of blocking cancer cell-derived glutamate in vivo in conjunction with currently used analgesics including NSAIDs such as meloxicam or clinically relevant opioids. These experiments will build on the findings of this report and others, furthering an understanding of the value of xCT as a therapeutic target for cancer pain.

Acknowledgment

The authors would like to thank Dr. Hanxin Lin (University of Western Ontario) for technical advice.

Author Contributions

Robert Ungard cultured cells for in vivo studies, induced the in vivo models, performed behavioral tests, and drafted the manuscript. Katja Linher-Melville performed qPCR, Western blotting, and cystine uptake assays for in vitro and in vivo studies; prepared cells for RNAseq; and contributed to writing and editing the manuscript. Manu Sharma assisted with all aspects of the in vivo studies. Jianping Wen generated and screened stable clones. Mina Nashed analyzed the RNAseq data. All authors contributed to successive drafts of the manuscript. Gurmit Singh supervised the overall project, edited the manuscript, and provided funding for the study. All authors have read and approved the final manuscript.

Declaration of Conflicting Interests

The author(s) declared no potential conflicts of interest with respect to the research, authorship, and/or publication of this article.

Funding

The author(s) disclosed receipt of the following financial support for the research, authorship, and/or publication of this article: This study was supported by grants to G. Singh from the Canadian Institutes of Health Research and the Canadian Breast Cancer Foundation and fellowships from the Canadian Institutes of Health Research and the Michael G. DeGroote Institute for Pain Research and Care to R. Ungard.

Supplemental material

Supplemental material is available for this article online.

References

1. Kennecke H, Yerushalmi R, Woods R, Cheang MCU, Voduc D, Speers CH, Nielsen TO and Gelmon K. Metastatic behavior of breast cancer subtypes. *J Clin Oncol* 2010; 28: 3271–3277.
2. Harries M, Taylor A, Holmberg L, Agbaje O, Garmo H, Kabilan S and Purushotham A. Incidence of bone metastases and survival after a diagnosis of bone metastases in breast cancer patients. *Cancer Epidemiol* 2014; 38: 427–434.
3. Coleman RE. Skeletal complications of malignancy. *Cancer* 1997; 80: 1588–1594.
4. Coleman RE and Rubens RD. The clinical course of bone metastases from breast cancer. *Br J Cancer* 1987; 55: 61–66.
5. Solomayer EF, Diel IJ, Meyberg GC, Gollan C and Bastert G. Metastatic breast cancer: clinical course, prognosis and therapy related to the first site of metastasis. *Breast Cancer Res Treat* 2000; 59: 271–278.
6. Yavas O, Hayran M and Ozisik Y. Factors affecting survival in breast cancer patients following bone metastasis. *Tumori* 2007; 93:580–586.
7. Bloom AP, Jimenez-Andrade JM, Taylor RN, Castañeda-Corral G, Kaczmarska MJ, Freeman KT, Coughlin KA, Ghilardi JR, Kuskowski MA and Mantyh PW. Breast cancer-induced bone remodeling, skeletal pain, and sprouting of sensory nerve fibers. *J Pain* 2011; 12: 698–711.
8. Wacnik PW, Baker CM, Herron MJ, Kren BT, Blazar BR, Wilcox GL, Hordinsky MK, Beitz AJ and Ericson ME. Tumor-induced mechanical hyperalgesia involves CGRP receptors and altered innervation and vascularization of DsRed2 fluorescent hindpaw tumors. *Pain* 2005; 115: 95–106.
9. Honore P, Rogers SD, Schwei MJ, Salak-Johnson JL, Luger NM, Sabino MC, Clohisy DR and Mantyh PW. Murine models of inflammatory, neuropathic and cancer pain each generates a unique set of neurochemical changes in the spinal cord and sensory neurons. *Neuroscience* 2000; 98: 585–598.
10. Schwei MJ, Honore P, Rogers SD, Salak-Johnson JL, Finke MP, Ramnaraine ML, Clohisy DR and Mantyh PW. Neurochemical and cellular reorganization of the spinal cord in a murine model of bone cancer pain. *J Neurosci* 1999; 19: 10886–10897.
11. Wang L-N, Yang J-P, Ji F-h, Zhan Y, Jin X-h, Xu Q-N, Wang X-Y and Zuo J-L. Brain-derived neurotrophic factor modulates N-methyl-D-aspartate receptor activation in a rat model of cancer-induced bone pain. *J Neurosci Res* 2012; 90: 1249–1260.
12. De Ciantis PD, Yashpal K, Henry J and Singh G. Characterization of a rat model of metastatic prostate cancer bone pain. *J Pain Res* 2010; 3: 213–221.
13. Ghilardi JR, Röhrich H, Lindsay TH, Sevcik MA, Schwei MJ, Kubota K, Halvorson KG, Poblete J, Chaplan SR, Dubin AE, Carruthers NI, Swanson D, Kuskowski M, Flores CM, Julius D and Mantyh PW. Selective blockade of the capsaicin receptor TRPV1 attenuates bone cancer pain. *J Neurosci* 2005; 25: 3126–3131.
14. Jimenez-Andrade JM, Ghilardi JR, Castañeda-Corral G, Kuskowski MA and Mantyh PW. Preventive or late administration of anti-NGF therapy attenuates tumor-induced nerve sprouting, neuroma formation, and cancer pain. *Pain* 2011; 152: 2564–2574.
15. Mantyh WG, Jimenez-Andrade JM, Stake JI, Bloom AP, Kaczmarska MJ, Taylor RN, Freeman KT, Ghilardi JR, Kuskowski MA and Mantyh PW. Blockade of nerve sprouting and neuroma formation markedly attenuates the development of late stage cancer pain. *Neuroscience* 2010; 171: 588–598.

16. Seidlitz EP, Sharma MK, Saikali Z, Ghert M and Singh G. Cancer cell lines release glutamate into the extracellular environment. *Clin Exp Metastasis* 2009; 26: 781–787.
17. Sharma MK, Seidlitz EP and Singh G. Cancer cells release glutamate via the cystine/glutamate antiporter. *Biochem Biophys Res Commun* 2010; 391: 91–95.
18. Zhu YF, Ungard R, Seidlitz E, Zacal N, Huizinga J, Henry JL, Singh G. Differences in electrophysiological properties of functionally identified nociceptive sensory neurons in an animal model of cancer-induced bone pain. *Mol Pain* 2016; 12: 1744806916628778.
19. Ungard RG, Seidlitz EP and Singh G. Inhibition of breast cancer-cell glutamate release with sulfasalazine limits cancer-induced bone pain. *Pain* 2014; 155: 28–36.
20. Slosky LM, BassiriRad NM, Symons AM, Thompson M, Doyle T, Forte BL, Staatz WD, Bui L, Neumann WL, Mantyh PW, Salvemini D, Largent-Milnes TM and Vanderah TW. The cystine/glutamate antiporter system xc− drives breast tumor cell glutamate release and cancer-induced bone pain. *Pain* 2016; 157: 2605–2616.
21. Fazzari J, Balenko M, Zacal N and Singh G. Identification of capsazepine as a novel inhibitor of system x_c^- and cancer-induced bone pain. *J Pain Res* 2017; 10: 915–925.
22. Miladinovic T, Ungard RG, Linher-Melville K, Popovic S and Singh G. Functional effects of TrkA inhibition on system x_C^--mediated glutamate release and cancer-induced bone pain. *Mol Pain* 2018; 14: 174480691877646.
23. Schmittgen TD and Livak KJ. Analyzing real-time PCR data by the comparative C(T) method. *Nat Protoc* 2008; 3: 1101–1108.
24. Zimmermann M. Ethical guidelines for investigations of experimental pain in conscious animals. *Pain* 1983; 16: 109–110.
25. Nashed MG, Linher-Melville K, Frey BN and Singh G. RNA-sequencing profiles hippocampal gene expression in a validated model of cancer-induced depression. *Genes Brain Behav* 2016; 15: 711–721.
26. Linher-Melville K, Nashed MG, Ungard RG, Haftchenary S, Rosa DA, Gunning PT, Singh G. Chronic inhibition of STAT3/STAT5 in treatment-resistant human breast cancer cell subtypes: convergence on the ROS/SUMO pathway and its effects on xCT expression and system xc-activity. *PLoS One* 2016; 11: e0161202.
27. Trapnell C, Roberts A, Goff L, Pertea G, Kim D, Kelley D R, Pimentel H, Salzberg S L, Rinn J L and Pachter L. Differential gene and transcript expression analysis of RNA-seq experiments with TopHat and Cufflinks. *Nat Protoc* 2012; 7: 562–578.
28. Lander ES and Waterman MS. Genomic mapping by fingerprinting random clones: a mathematical analysis. *Genomics* 1988; 2: 231–239.
29. Huang DW, Sherman BT and Lempicki RA. Systematic and integrative analysis of large gene lists using DAVID bioinformatics resources. *Nat Protoc* 2009; 4: 44–57.
30. Huang DW, Sherman BT and Lempicki RA. Bioinformatics enrichment tools: paths toward the comprehensive functional analysis of large gene lists. *Nucleic Acids Res* 2009; 37: 1–13.
31. Livak KJ and Schmittgen TD. Analysis of relative gene expression data using real-time quantitative PCR and the 2(-Delta Delta C(T)) Method. *Methods* 2001; 25: 402–408.
32. Zhen AW, Nguyen NH, Gibert Y, Motola S, Buckett P, Wessling-Resnick M, Fraenkel E and Fraenkel PG. The small molecule, genistein, increases hepcidin expression in human hepatocytes. *Hepatology* 2013; 58: 1315–1325.
33. Habib E, Linher-Melville K, Lin H-X and Singh G. Expression of xCT and activity of system xc− are regulated by NRF2 in human breast cancer cells in response to oxidative stress. *Redox Biol* 2015; 5: 33–42.
34. Linher-Melville K, Zantinge S, Sanli T, Gerstein H, Tsakiridis T and Singh G. Establishing a relationship between prolactin and altered fatty acid β-Oxidation via carnitine palmitoyl transferase 1 in breast cancer cells. *BMC Cancer* 2011; 11: 56.
35. Linher-Melville K, Haftchenary S, Gunning P and Singh G. Signal transducer and activator of transcription 3 and 5 regulate system Xc- and redox balance in human breast cancer cells. *Mol Cell Biochem* 2015; 405: 205–221.
36. Wang X, Spandidos A, Wang H and Seed B. PrimerBank: a PCR primer database for quantitative gene expression analysis, 2012 update. *Nucleic Acids Res* 2012; 40: D1144–D1149.
37. Coleman RE. Clinical features of metastatic bone disease and risk of skeletal morbidity. *Clin Cancer Res* 2006; 12: 6243s–6249s.
38. Timmerman LA, Holton T, Yuneva M, Louie RJ, Padró M, Daemen A, Hu M, Chan DA, Ethier SP, van 'T Veer LJ, Polyak K, McCormick F and Gray JW. Glutamine Sensitivity Analysis Identifies the xCT Antiporter as a Common Triple-Negative Breast Tumor Therapeutic Target. *Cancer Cell* 2013; 24: 450–465.
39. Huang Y and Sadée W. Membrane transporters and channels in chemoresistance and -sensitivity of tumor cells. *Cancer Lett* 2006; 239: 168–182.
40. Chung WJ, Lyons SA, Nelson GM, Hamza H, Gladson CL, Gillespie GY and Sontheimer H. Inhibition of cystine uptake disrupts the growth of primary brain tumors. *J Neurosci* 2005; 25: 7101–7110.
41. Fazzari J, Linher-Melville K and Singh G. Tumour-derived glutamate: linking aberrant cancer cell metabolism to peripheral sensory pain pathways. *Curr Neuropharmacol* 2017; 15: 620–636.
42. Cowan RW, Seidlitz EP and Singh G. Glutamate signaling in healthy and diseased bone. *Front Endocrinol (Lausanne)* 2012; 3: 89.
43. Orr FW, Lee J, Duivenvoorden WC and Singh G. Pathophysiologic interactions in skeletal metastasis. *Cancer* 2000; 88: 2912–2918.
44. Mach DB, Rogers SD, Sabino MC, Luger NM, Schwei MJ, Pomonis JD, Keyser CP, Clohisy DR, Adams DJ, O'Leary P and Mantyh PW. Origins of skeletal pain: sensory and sympathetic innervation of the mouse femur. *Neuroscience* 2002; 113: 155–166.
45. Lozano-Ondoua AN, Symons-Liguori AM and Vanderah TW. Cancer-induced bone pain: mechanisms and models. *Neurosci Lett* 2013; 557: 52–59.

46. Mantyh PW, Clohisy DR, Koltzenburg M and Hunt SP. Molecular mechanisms of cancer pain. *Nat Rev Cancer* 2002; 2: 201–209.
47. Jackman NA, Uliasz TF, Hewett JA and Hewett SJ. Regulation of system x(c)(-)activity and expression in astrocytes by interleukin-1β: implications for hypoxic neuronal injury. *Glia* 2010; 58: 1806–1815.
48. Shi J, He Y, Hewett SJ and Hewett JA. Interleukin 1β regulation of the system xc- substrate-specific subunit, xCT, in primary mouse astrocytes involves the RNA-binding protein HuR. *J Biol Chem* 2016; 291: 1643–1651.
49. Oliveira A, Dinis-Oliveira RJ, Nogueira A, Gonçalves F, Silva P, Vieira C, Silvestre R, Carvalho F and Medeiros R. Interleukin-1β genotype and circulating levels in cancer patients: metastatic status and pain perception. *Clin Biochem* 2014; 47: 1209–1213.
50. Reyes-Gibby CC, Swartz MD, Yu X, Wu X, Yennurajalingam S, Anderson KO, Spitz MR and Shete S. Symptom clusters of pain, depressed mood, and fatigue in lung cancer: assessing the role of cytokine genes. *Support Care Cancer* 2013; 21: 3117–3125.
51. Chitu V and Stanley ER. Colony-stimulating factor-1 in immunity and inflammation. *Curr Opin Immunol* 2006; 18: 39–48.
52. De I, Nikodemova M, Steffen MD, Sokn E, Maklakova VI, Watters JJ and Collier LS. CSF1 overexpression has pleiotropic effects on microglia *in vivo*. *Glia* 2014; 62: 1955–1967.
53. Reyes-Gibby CC, Spitz MR, Yennurajalingam S, Swartz M, Gu J, Wu X, Bruera E and Shete S. Role of inflammation gene polymorphisms on pain severity in lung cancer patients. *Cancer Epidemiol Biomarkers Prev* 2009; 18: 2636–2642.
54. Robert SM, Buckingham SC, Campbell SL, Robel S, Holt KT, Ogunrinu-Babarinde T, Warren PP, White DM, Reid MA, Eschbacher J M, Berens ME, Lahti AC, Nabors LB and Sontheimer H. SLC7A11 expression is associated with seizures and predicts poor survival in patients with malignant glioma. *Sci Transl Med* 2015; 7: 289ra86.
55. Nashed MG, Ungard RG, Young K, Zacal NJ, Seidlitz EP, Fazzari J, Frey BN, Singh G. Behavioural effects of using sulfasalazine to inhibit glutamate released by cancer cells: A novel target for cancer-induced depression. *Sci Rep* 2017; 7: 41382.